New experimental measurement of ^{nat}Se(n, γ) cross section between 1 eV to 1 keV at the CSNS Back-n facility

Xin-Rong Hu(胡新荣), Long-Xiang Liu(刘龙祥), Wei Jiang(蒋伟), Jie Ren(任杰), Gong-Tao Fan(范功涛), Hong-Wei Wang(王宏伟), Xi-Guang Cao(曹喜光), Long-Long Song(宋龙龙), Ying-Du Liu(刘应都), Yue Zhang(张岳), Xin-Xiang Li(李鑫祥), Zi-Rui Hao(郝子锐), Pan Kuang(匡攀), Xiao-He Wang(王小鹤), Ji-Feng Hu(胡继峰), Bing Jiang(姜炳), De-Xin Wang(王德鑫), Suyalatu Zhang(张苏雅拉吐), Zhen-Dong An(安振东), Yu-Ting Wang(王玉廷), Chun-Wang Ma(马春旺), Jian-Jun He(何建军), Jun Su(苏俊), Li-Yong Zhang(张立勇), Yu-Xuan Yang(杨宇萱), Sheng Jin(金晟), and Kai-Jie Chen(陈开杰)

Citation: Chin. Phys. B, 2022, 31 (**8**): 080101. DOI: 10.1088/1674-1056/ac6ee2
Journal homepage: http://cpb.iphy.ac.cn; http://iopscience.iop.org/cpb

What follows is a list of articles you may be interested in

Measurement of ^{232}Th (n,γ) cross section at the CSNS Back-n facility in the unresolved resonance region from 4 keV to 100 keV

Bing Jiang(姜炳), Jianlong Han(韩建龙), Jie Ren(任杰), Wei Jiang(蒋伟), Xiaohe Wang(王小鹤), Zian Guo(郭子安), Jianglin Zhang(张江林), Jifeng Hu(胡继峰), Jingen Chen(陈金根), Xiangzhou Cai(蔡翔舟), Hongwei Wang(王宏伟), Longxiang Liu(刘龙祥), Xinxiang Li(李鑫祥), Xinrong Hu(胡新荣), and Yue Zhang(张岳)

Chin. Phys. B, 2022, 31 (**6**): 060101. DOI: 10.1088/1674-1056/ac5394

Detailed calibration of the PI-LCX: 1300 high performance single photon counting hard x-ray CCD camera

Wei Hong(洪伟), Xian-Lun Wen(温贤伦), Lai Wei(魏来), Bin Zhu(朱斌), Yu-Chi Wu(吴玉迟), Ke-Gong Dong(董克攻), Chun-Ye Jiao(焦春晔), Bo Wu(伍波), Ying-Ling He(何颖玲), Fa-Qiang Zhang(张发强), Wei-Min Zhou(周维民), Yu-Qiu Gu(谷渝秋)

Chin. Phys. B, 2017, 26 (**2**): 025204. DOI: 10.1088/1674-1056/26/2/025204

Spectral and ion emission features of laser-produced Sn and SnO_2 plasmas

Hui Lan(兰慧), Xin-Bing Wang(王新兵), Du-Luo Zuo(左都罗)

Chin. Phys. B, 2016, 25 (**3**): 035202. DOI: 10.1088/1674-1056/25/3/035202

Simulations of the L–H transition dynamics with different heat and particle sources

Li Hui-Dong, Wang Zhan-Hui, Jan Weiland, Feng Hao, Sun Wei-Guo

Chin. Phys. B, 2015, 24 (**11**): 115204. DOI: 10.1088/1674-1056/24/11/115204

Compound sawtooth in EAST LHCD plasma： An experimental study

Xu Li-Qing, Hu Li-Qun, Chen Kai-Yun, Li Miao-Hui

Chin. Phys. B, 2014, 23 (**8**): 085201. DOI: 10.1088/1674-1056/23/8/085201

DATA PAPER

New experimental measurement of ^{nat}Se(n, γ) cross section between 1 eV to 1 keV at the CSNS Back-n facility

Xin-Rong Hu(胡新荣)[1,2], Long-Xiang Liu(刘龙祥)[3,†], Wei Jiang(蒋伟)[4,5], Jie Ren(任杰)[6], Gong-Tao Fan(范功涛)[2,3,1,‡], Hong-Wei Wang(王宏伟)[2,3,1,§], Xi-Guang Cao(曹喜光)[3,1], Long-Long Song(宋龙龙)[3], Ying-Du Liu(刘应都)[7], Yue Zhang(张岳)[4,5], Xin-Xiang Li(李鑫祥)[1,2], Zi-Rui Hao(郝子锐)[1,2], Pan Kuang(匡攀)[1,2], Xiao-He Wang(王小鹤)[1], Ji-Feng Hu(胡继峰)[1], Bing Jiang(姜炳)[1,2], De-Xin Wang(王德鑫)[8], Suyalatu Zhang(张苏雅拉吐)[8], Zhen-Dong An(安振东)[9], Yu-Ting Wang(王玉廷)[10], Chun-Wang Ma(马春旺)[10], Jian-Jun He(何建军)[11], Jun Su(苏俊)[11], Li-Yong Zhang(张立勇)[11], Yu-Xuan Yang(杨宇萱)[1,12], Sheng Jin(金晟)[1,2], and Kai-Jie Chen(陈开杰)[1,13]

[1] *Shanghai Institute of Applied Physics, Chinese Academy of Sciences, Shanghai* 201800, *China*
[2] *University of Chinese Academy of Sciences, Beijing* 100049, *China*
[3] *Shanghai Advanced Research Institute, Chinese Academy of Sciences, Shanghai* 201210, *China*
[4] *Institute of High Energy Physics, Chinese Academy of Sciences, Beijing* 100049, *China*
[5] *Spallation Neutron Source Science Center, Dongguan* 523803, *China*
[6] *Key Laboratory of Nuclear Data, China Institute of Atomic Energy, Beijing* 102413, *China*
[7] *Xiangtan University, Xiangtan* 411105, *China*
[8] *Institute of Nuclear Physics, Inner Mongolia University for the Nationalities, Tongliao* 028000, *China*
[9] *Sun Yat-sen University, Zhuhai* 510275, *China*
[10] *Henan Normal University, Xinxiang* 453007, *China*
[11] *Beijing Normal University, Beijing* 100875, *China*
[12] *School of Physics and Microelectronics, Zhengzhou University, Zhengzhou 450052, China*
[13] *ShanghaiTech University, Shanghai* 200120, *China*

(Received 7 March 2022; revised manuscript received 28 April 2022; accepted manuscript online 12 May 2022)

The ^{74}Se is one of 35 p-nuclei, and ^{82}Se is a r-process only nucleus, and their (n, γ) cross sections are vital input parameters for nuclear astrophysics reaction network calculations. The neutron capture cross section in the resonance range of isotopes and even natural selenium samples has not been measured. Prompt γ-rays originating from neutron-induced capture events were detected by four C_6D_6 liquid scintillator detectors at the Back-n facility of China Spallation Neutron Source (CSNS). The pulse height weighting technique (PHWT) was used to analyze the data in the 1 eV to 100 keV region. The deduced neutron capture cross section was compared with ENDF/B-VIII.0, JEFF-3.2, and JENDL-4.0, and some differences were found. Resonance parameters were extracted by the *R*-matrix code SAMMY in the 1 eV–1 keV region. All the cross sections of ^{nat}Se and resonance parameters are given in the datasets. The datasets are openly available at http://www.doi.org/10.11922/sciencedb.j00113.00019.

Keywords: ^{nat}Se (n,γ) cross section, CSNS Back-n facility, C_6D_6 detectors, resolved resonance region, *R*-matrix

PACS: 01.52.+r, 24.30.–v, 29.25.Dz, 52.70.La **DOI:** 10.1088/1674-1056/ac6ee2

1. Introduction

Most of the elements heavier than iron in the universe are mainly formed by the slow neutron capture process (s-process)[1,2] and the rapid neutron capture process (r-process).[3] which account for about 50% of the whole stable elements respectively.[4] The rest of elements heavier than iron, about 1%, are produced by the capture of charged particles (p, γ) and the photonuclear reaction (γ, n), which is called p-process, and eventually produces the stable proton rich p-nuclei.[5] The study of these nuclides and the accurate measurement of Maxwellian averaged cross section (MACS) of related nuclides for neutron capture reactions are of great significance in nuclear astrophysics.[6] The s-process mainly occurs in asymptotic giant branch (AGB) stars, in which the neutron density is low. The unstable sub-nuclei of the s-process form stable isobars through β-decay, and then continue to form new nuclide by means of additional neutron capture processes. Therefore, the slow neutron capture process takes place mainly along the β stable line. The r-process mainly occurs in supernova explosion or neutron star mergers. Due to the extreme neutron densities ($\sim 10^{20}$ cm^{-3}) and short time scales ($\sim$ 10 s),[7] very neutron rich nuclei are formed, which even-

†Corresponding author. E-mail: liulongxiang@zjlab.org.cn
‡Corresponding author. E-mail: fangongtao@zjlab.org.cn
§Corresponding author. E-mail: wanghongwei@zjlab.org.cn

tually decay through a series of beta decays.

Se is one of the key elements in nuclear astrophysics research. Isotopes of Se are in the path of slow neutron capture process. The (n, γ) cross sections of Se isotopes, help to determine the abundance of the related elements in the universe. The slow neutron capture process in the Se-region is presented in Fig. 1. The accurate measurements of the neutron capture cross sections of Se isotopes play an essential role in the reaction network of the nuclear astrophysics. According to the different properties of Se isotopes, measurements of neutron capture cross section of Se isotopes follow different methods. ^{79}Se, with a half-life of 295 ky, is one of the long-lived fission products (LLFPs) for which neutron capture cross section is important from the viewpoint of nuclear power.[8] Besides, ^{79}Se is an important branching point in the s-process path. However, there are no direct measurement neutron capture cross section data because it is difficult to obtain samples of ^{79}Se. The ^{79}Se (n, γ) cross section was constrained by its reverse reaction of ^{80}Se (γ, n) by the laser Compton scattering gamma source (LCS-γ) in 2009.[9] The neutron capture cross section of the other six stable isotopes can be directly measured via (n, γ) reaction. The natural abundances of the stable Se isotopes are 0.89%, 9.37%, 7.63%, 23.77%, 49.61%, and 8.73% for ^{74}Se, ^{76}Se, ^{77}Se, ^{78}Se, ^{80}Se, and ^{82}Se, respectively. In which,^{74}Se is a p-nucleus, synthesized by the p-process, and its abundance is only 0.86%; ^{76,77,78,80}Se isotopes are mainly produced by the s-process, while ^{82}Se is produced by the r-process.

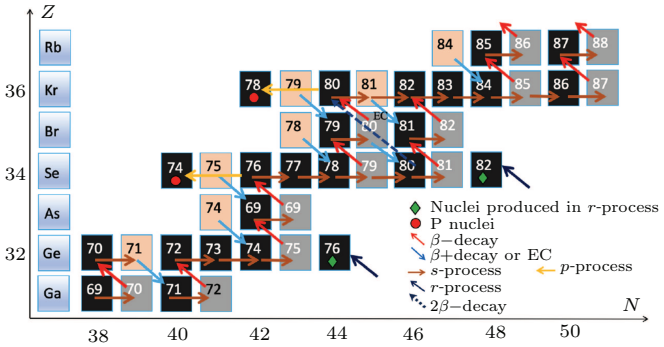

Fig. 1. Synthetic network diagram of nuclei near Se isotopes. The black boxes represent stable nuclei, the orange boxes represent unstable nuclei that can undergo $\beta+$ decay, and the gray boxes represent $\beta-$ decay nuclei; The red arrows represent $\beta-$ decay, the blue arrows represent $\beta+$ decay, the dark yellow arrows represent s-process, the yellow arrows represent p-process, and the dark blue arrows represent r-process.

Until now, there has not been enough experimental neutron capture cross sections for the selenium element in the 1 eV–1 keV resolved resonance region, except keV-region's MACS for ^{76}Se[10] and ^{78}Se[11] isotopes. Recently, Babiano-Suarez *et al.*[12] measured the ^{80}Se (n, γ) cross section at n_TOF in 2020, gave some resonance peak in the energy range from 0.1 keV to 100 keV but without *R*-matrix analysis. This work is the first experimental measurement of neutron capture cross section of natural selenium in the energy region between 1 eV and 1 keV at Back-n facility in CSNS. The experimental methods and data processing are analyzed in detail below. Finally, the neutron capture resonance parameters of ^{nat}Se are also given.

2. Experimental setup

2.1. The Back-n facility

The neutron time-of-flight facility Back-n is one of the neutron beam lines in China Spallation Neutron Source (CSNS), which can provide continuous neutron energy spectrum in the energy range from 0.1 eV to 200 MeV. CSNS is the first spallation neutron source in China.[13] Here, neutrons are produced by a pulse proton beam with an energy of 1.6 GeV and a repetition frequency of 25 Hz, bombarding a tungsten–tantalum (W–Ta) target. The proton pulse of CSNS can be divided into three operation modes: i) the narrow beam bunch with the proton bunch width of 3.7 ns; ii) the single bunch mode, the bunch time structure is parabolic shape with bunch width of 60 ns; iii) the double-bunch mode, which consists of two single-bunch protons with a spacing of 410 ns. The measurement of neutron capture cross section in the resonance energy region is carried out under the double-bunch mode. The Back-n white neutron source is built at the back-scattering direction of the proton beam, which mainly focuses on nuclear data measurements and detector calibration. This beamline has two experiment stations ES1 and ES2 with the distances of 55 m and 76 m from the spallation target to each station, respectively. ES1 mainly studies the (n, light charge particle (lcp)) reaction cross section, and ES2 is mainly for the measurement of (n, γ), (n, tot), and (n, f) reaction cross sections. Our measurement is carried out at ES2. More detailed information on the Back-n facility can be found in Refs. [14–19].

2.2. The C_6D_6 detectors

Four deuterated benzene (C_6D_6) liquid scintillator detectors were used for the γ-ray detection. The C_6D_6 detectors were placed upstream of the neutron beam sample to reduce the scattering neutron background. The main advantages of these detectors are a fast time response, with pulse width of the order 10 ns, and a very low sensitivity to scattered neutrons, which are widely used for (n, γ) cross section measurements up to now. The shell of the scintillator is made of aluminum due to its low capture rate, with a diameter and length of 130 mm and 76.2 mm, respectively. The distance between the detector center to the sample centre is about 150 mm, and the distance from the neutron beam centre to the centre of the front face of the detector is about 80 mm.[20] Figure 2 shows the Geant4 geometry of the sample and detectors implemented for this experiment.

Fig. 2. A schematic view of the detectors and sample setup used for this experiment by Geant4 simulation.

In the neutron capture cross section measurements, the amplitudes of the anode signals of the C_6D_6 detectors range from 0.01 V to 3 V. Signals from the C_6D_6 detectors are delivered to flash ADCs, which can digitize the signals into a full waveform with a 1 GS/s sampling rate and 12 bits resolution.[21] The incident neutron energy was determined by the time-of-flight (TOF) technique. The neutron energy E_n is given by Eq. (1) and the corresponding neutron resolution is presented by Eq. (2),[24]

$$E_n = \frac{1}{2}m_n v^2 = \left(\frac{72.2977L}{T_f}\right)^2, \tag{1}$$

$$\frac{\Delta E_n}{E_n} = 2\sqrt{\left(\frac{\Delta L}{L}\right)^2 + \left(\frac{\Delta T_f}{T_f}\right)^2}, \tag{2}$$

where the neutron flight length $L = L_0 + \Delta L(E_n)$, L_0 is the geometric distance from the spallation target to the experimental sample, and $\Delta L(E_n)$ is the equivalent change in moderation length associated with the incident neutron energy. T_f is the neutron time of flight, given by $T_f = t_n - t_\gamma + L/c$, where t_n and t_γ are the start time of the neutron capture signal and the start time of the gamma flash recorded by the data acquisition (DAQ) system, respectively; c is the speed of light.

Besides, the neutron flux was measured by using a silicon monitor; and the silicon monitor consists of a thin ^{6}LiF conversion layer and eight silicon detectors outside the neutron beam (Li–Si monitor) to count the number of neutrons by detecting alpha particles and ^{3}H through the reaction ^{6}Li (n, α)^{3}H.[22] It is worth mentioning that with this detection system we have measured the neutron capture cross section of ^{197}Au[28] and ^{nat}Er[29] successfully, which validated the performance of the detection system and the processing methodology.

2.3. Samples

The ^{nat}Se sample consisted of selenium monomers in powder form with a purity of 99.99%. In addition, the natural carbon sample and empty holder were used for the neutron scattering background and surroundings γ-ray background subtraction, the ^{nat}Pb sample for in-beam γ-ray background. Data were also recorded with a ^{197}Au sample for normalizing the cross section using 4.9 eV resonance for the saturated resonance method.[23] Table 1 shows the properties of the samples used in the experiment. The ^{nat}Se sample was measured for 80 hours with a proton power between 22.8 kW and 23.4 kW. Then the gold sample and carbon sample were measured for 12 hours respectively, and finally the empty target was measured for 10 hours with a proton power 31.2–33.4 kW.

Table 1. Properties of the samples used in the measurement.

Sample	Formula	Mass (g)	Diameter (mm)	Thickness (mm)	Area density (atom/barn)
^{nat}Se	Se > 99.99% Pb = 4 ppm Cu = 9 ppm Fe = 17 ppm Sn = 8 ppm Al = 19 ppm As = 7 ppm Sb = 6 ppm Ni = 11 ppm Bi = 8 ppm	18.89±0.02	50±1	2.00±0.02	7.304×10^{-3}
^{nat}C	> 99.90%	4.42±0.02	50±1	1.00 ±0.02	1.128×10^{-2}
^{197}Au	> 99.90%	37.93±0.03	50±1	1.00 ±0.02	5.907×10^{-3}
^{nat}Pb	> 99.90%	4.24±0.01	30±1	0.53 ±0.01	1.748×10^{-3}

3. Data analysis

3.1. Pluse height weighting technique

The C_6D_6 detection system is one of the total energy detection system that is widely used for neutron capture cross section measurements. In 1963, Moxon and Rae[25] first proposed the principle of the pulse height weighting technology (PHWT), then Macklin and Gibbons[26] for the first time used this method to measure the neutron capture cross section in 1967. PHWT has been developed for decades and has become a mature neutron capture cross section measurement method. According to this technique, two conditions must be met. First, the detection efficiency to gamma-rays has to be so low that at most only one gamma ray is detected in a capture event. Second, the detection efficiency is directly proportional to the energy of the gamma, $\varepsilon_\gamma = k \cdot E_\gamma$. Owing to $\varepsilon_\gamma \ll 1$ and $E_c = E_n + S_n$, the capture efficiency ε_c can be written as[27]

$$\varepsilon_c = 1 - \prod_{i=1}^{m}(1-\varepsilon_{\gamma_i}) \simeq \sum_{i=1}^{m}\varepsilon_{\gamma_i} = k\sum_{i=1}^{m}E_{\gamma_i} = k\cdot(E_n + S_n). \tag{3}$$

However, the response of the detectors to gamma-rays is not linear with the gamma energy, resulting in different detection efficiency ($\varepsilon_c(E_n)$) of capture events in different de-excitation paths. In order to meet the second condition, the weighting function (WF) $W(E_i)$ can be introduced as follows:

$$W(E_i) = \sum_{k=0}^{4} a_k {E_i}^k. \tag{4}$$

The weighting function $W(E_i)$ was taken as a fourth order polynomial $\sum_{k=0}^{4} a_k E_i^k$ of which the coefficients a_k were determined by likelihood maximization (Eq. (5)) using the simulated detector system response function (shown in Fig. 3(a)) to several monoenergetic gamma-rays,

$$\chi^2 = \sum_j \left[kE_{\gamma j} - \int_{E_L}^{\infty} R\left(E_d, E_{\gamma j}\right) W\left(E_d\right) \mathrm{d}E_d \right]^2 . \quad (5)$$

Usually, the coefficient k is set to one, and $R\left(E_d, E_{\gamma j}\right)$ is the response function of the detectors of the j_{th} γ-rays with an energy of $E_{\gamma j}$ from the Geant4 simulation. The detailed geometry in these simulations includes the sample, sample holder, and detector. The simulated γ-rays with energy ranging from 0.15 MeV to 11 MeV were produced from the Se sample, then emitted homogeneously, and partial gamma-rays were deposited energy in the C_6D_6 detectors. Figure 3(b) shows that the original detection efficiency of the primary C_6D_6 setup is approximately 2%, the weighted efficiency is proportional to the γ-rays energy, and the ratios between the weighted efficiency and gamma energy of each energy point are very close to one.

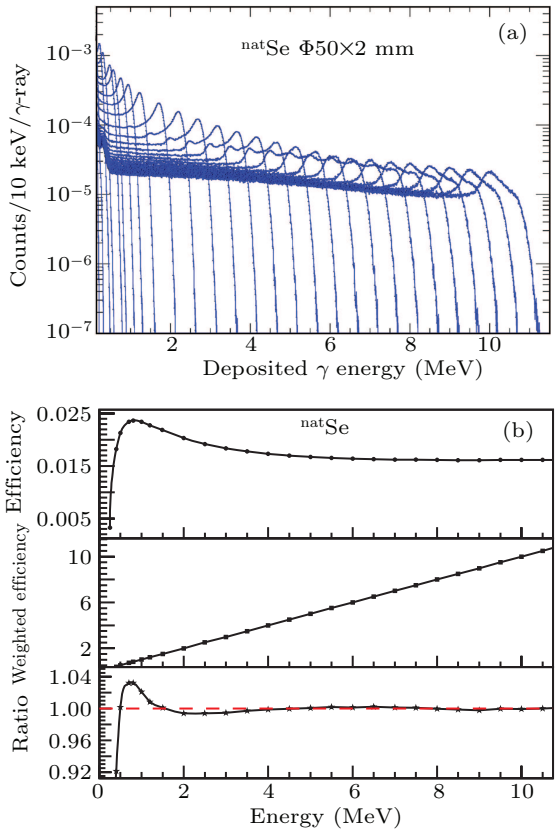

Fig. 3. (a) The response function of the C_6D_6 detectors of $^{\mathrm{nat}}$Se simulated by Geant4 with energy broadening. (b) The original efficiency of the C_6D_6 detectors in the top tile, the weighted efficiency of the detectors shown in the middle tile, and the ratio between weighted efficiency and the corresponding γ energy in the bottom tile, which is very close to one.

3.2. Determination of the capture yield

The experimental capture yield Y_W[30,31] has been extracted dividing the weighted counts C_W, after subtraction of the total background B_W, by the incident neutron fluence ϕ_n:

$$Y_W(E_n) = f_N \times \frac{C_W(E_n) - B_W(E_n)}{\phi_n(E_n) \times \varepsilon_{E_n}}, \quad (6)$$

where f_N is the normalization factor, which was obtained from the measurement of the saturated 4.9 eV resonance in the thick ^{197}Au sample. ε_{E_n} is the detection efficiency, which for weighted counts is equal to the excitation energy $(S_n + E_n)$ according to Eq. (3), and $S_n = 7.054$ MeV for $^{\mathrm{nat}}$Se. C_W and B_W are the weighted pulse height spectra for the $^{\mathrm{nat}}$Se sample and the total background, respectively. The neutron fluence was measured with the Li–Si detector, while above 10 keV it was measured with a U-235 fission chamber. More details can be found in Ref. [32].

The neutron capture yield is the probability for an incident neutron to undergo a capture reaction, which is related to the capture σ_γ and total cross section σ_{tot}. Considering the neutron self-absorption, we have

$$Y(E_n) = (1 - \mathrm{e}^{-n\sigma_{\mathrm{tot}}}) \frac{\sigma_\gamma}{\sigma_{\mathrm{tot}}}, \quad (7)$$

where n represents the sample's areal density. Combining Eqs. (6) and (7), we can give the experimental neutron capture cross sections, where σ_{tot} are taken from ENDF/B-VIII.0.

3.3. Background estimation

A number of background contributions to the observed counts were identified and are shown in Fig. 4 along with the measured spectrum of the $^{\mathrm{nat}}$Se sample. Their contributions were the ambient background subtracted by the empty holder, neutron scattering background from sample subtracted by the carbon sample, and in-beam γ-ray background deduced by the lead sample. The whole samples have been normalized by the Li–Si monitor shown in Fig. 4. Because the $^{\mathrm{nat}}$Pb sample has high gamma scattering cross section and low neutron scattering cross section, it was used for in-beam gamma calibration. It can be seen that the in-beam gamma mainly contributes to the energy region above 100 eV. The background contribution in the low energy band from the $^{\mathrm{nat}}$Pb sample was less than the empty sample background contributions as shown in Fig. 4. The total background $B(E_n)$ was expressed as following formula:

$$\begin{aligned} B(E_n) &= B_0 + B_{\mathrm{em}}(E_n) + B_{\mathrm{ns}}(E_n) + B_{\gamma s}(E_n) \\ &= N_{\mathrm{empty}} + \eta\left(N_C - N_{\mathrm{empty}}\right) + \left(N_{\mathrm{Pb}} - N_{\mathrm{empty}}\right), \end{aligned} \quad (8)$$

where B_0 is the time-independent background that mainly comes from the natural environment, $B_{\mathrm{em}}(E_n)$ is the sample-independent background originating from the neutron beam flux with anything other than the $^{\mathrm{nat}}$Se sample, $B_{\mathrm{ns}}(E_n)$ is the background caused by the neutron scattered from the sample, $B_{\gamma s}(E_n)$ is the background attributed to in-beam γ-rays scattering from the the $^{\mathrm{nat}}$Se sample; and η is the ratio of the product

of the neutron elastic scattering cross section and the number of nuclei per unit area of the ^{nat}Se sample to that of the carbon sample.

3.4. Uncertainty analysis

The experimental uncertainty of this work comes from the recent experiment conditions and data analysis. According to the Back-n collaboration's work,[32] the uncertainty of the neutron energy spectrum varies between 2.3% and 4.5% above 0.15 MeV and less than 8% below 0.15 MeV. The uncertainty from the proton beam power was recorded during the measurement, contributing an error of 2.0%. Uncertainty in data analysis mainly concluded the PHWT method, normalization and background subtraction. The system uncertainty of PHWT was 2.0%–3.0% according to Tain *et al.*[33] The systematic uncertainties from different sources contributing to the resulting yield normalization are summarized in Table 2. Owing to the diameter of samples (50 mm) larger than the neutron flux diameter (30 mm), the uncertainty caused by the relative position Se/Au is negligible. The uncertainty of the normalized factor of the gold sample at the saturated resonance energy of 4.9 eV is about 1%. According to J. Ren *et al.*,[34] there is an obvious in-beam gamma background at time-of-flight between 20 μs and 400 μs, namely, the keV energy region. The whole uncertainties are presented in Table 2.

Table 2. The statistic uncertainty and systematic uncertainties of this experiment.

σ	Meaning	Value
	Experiment conditions	
σ_{ϕ_1}	uncertainty of neutron energy spectrum below 0.15 MeV	< 8.0%
σ_{ϕ_2}	uncertainty of neutron energy spectrum above 0.15 MeV	< 4.5%
$\sigma_{\text{BeamPower}}$	uncertainty of proton beam power	< 3.5%
	Data analysis	
σ_{PHWT}	uncertainty from PHWT	< 3.0%
$\sigma_{\text{Normalized}}$	uncertainty of normalization	1.0%
	Statistical error	
$\sigma_{\text{Statistic}}$	statistic uncertainty	< 2.0%

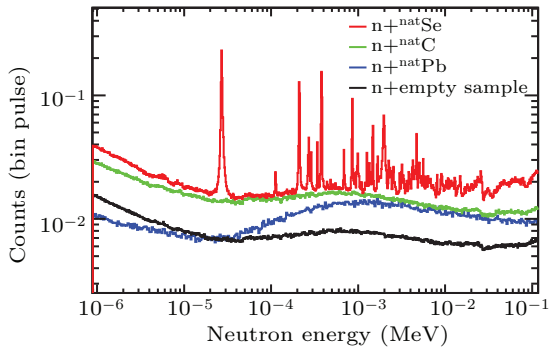

Fig. 4. The measured ^{nat}Se spectrum together with the various measured scaled background components has been normalized by a Li–Si monitor; and the count rates are expressed in a width-independent logarithmic equidistant binning.

4. Result and discussion

It is worth mentioning that the neutron capture cross sections of natural Se can be calculated by weighting the cross sections of Se isotopes according to their abundances. Figure 5 shows the neutron capture cross sections of ^{nat}Se and the contributions of Se isotopes in the energy region of 1 eV–100 keV respectively. The Se isotopes capture cross sections are taken from the ENDF/B-VIII.0 evaluation database.[35] We also plot the existing experimental data of ^{nat}Se neutron capture cross section in Fig. 5. In Fig. 5 one can see that the current experimental cross sections for neutron capture in Se isotopes are seriously deficient, and there are only few experimental results in the energy range below 100 keV.

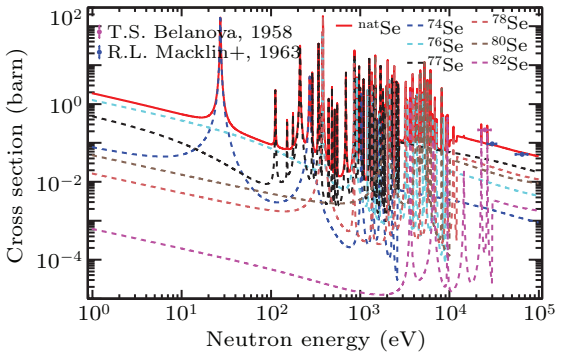

Fig. 5. The neutron caption cross section of ^{nat}Se is calculated by weighting the different isotopes cross sections with their abundances, where the red solid line represents the ^{nat}Se(n, γ) cross section and the dashed lines are the contributions of each isotope capture cross section. The magenta and blue solid dots represent the existing experimental data.

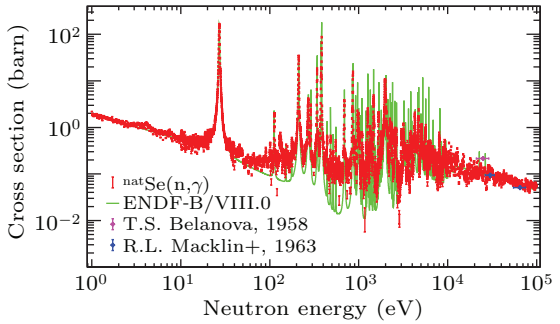

Fig. 6. The neutron capture cross section of ^{nat}Se in the energy region from 1 eV to 100 keV.

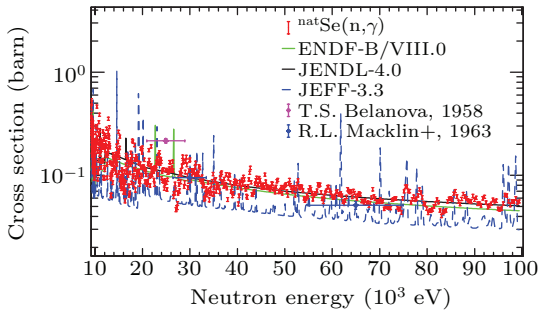

Fig. 7. The neutron capture cross section of ^{nat}Se in the unresolved resonance region from 10 keV to 100 keV.

This work measured the neutron capture cross section of ^{nat}Se in the 1 eV to 100 keV energy region, as shown in Fig. 6, where the red dots are the current experimental data and can roughly match the evaluated data ENDF/B-VIII.0[35] (green solid line). Figure 7 shows the neutron capture cross

section of ^{nat}Se in the unresolved resonance region (URR) of 10–100 keV, where the evaluation data JEFF-3.3.[37] shows a large number of resonance peaks in this energy region, which differs significantly from our experimental data. Compared with the ENDF/B-VIII.0 data, our results are in better agreement with the evaluated data JENDL-4.0,[36] which also verify the reasonableness of the experimental data. And in this region, there are only three previous experimental data points from R. L. Mackin *et al.*[39] and T. S. Belanova.[40] Considering there being a large in-beam gamma background,[34] it is difficult to subtract completely the whole background limited to the current experiment conditions. On the other hand, the white neutron source (WNS) used the double-bunch mode of proton pulse, which limits the neutron energy resolution in the energy region of above 1 keV. For the above reasons, there are large errors in the experimental data in the resolved resonance region (RRR) above 1 keV, and unfortunately the resonance analysis cannot be performed in this region. This work focuses on the analysis of the resonance parameters of ^{nat}Se in the 1 eV–1 keV energy region. Among them, the experimental results in the 100 eV to 1 keV energy region are compared with the ENDF/B-VIII.0 evaluation data as shown in Fig. 8, and overall, the experimental data can match the evaluation data well. The individual peak positions that are not matched, e.g., at 130 eV, are brought about by the neutron energy spectrum[28] structure.

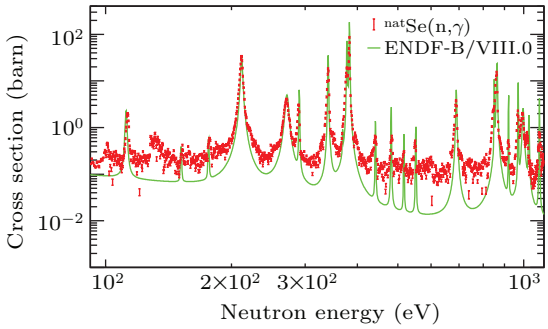

Fig. 8. The neutron capture cross section of ^{nat}Se in resonance regions of 0.1–1 keV.

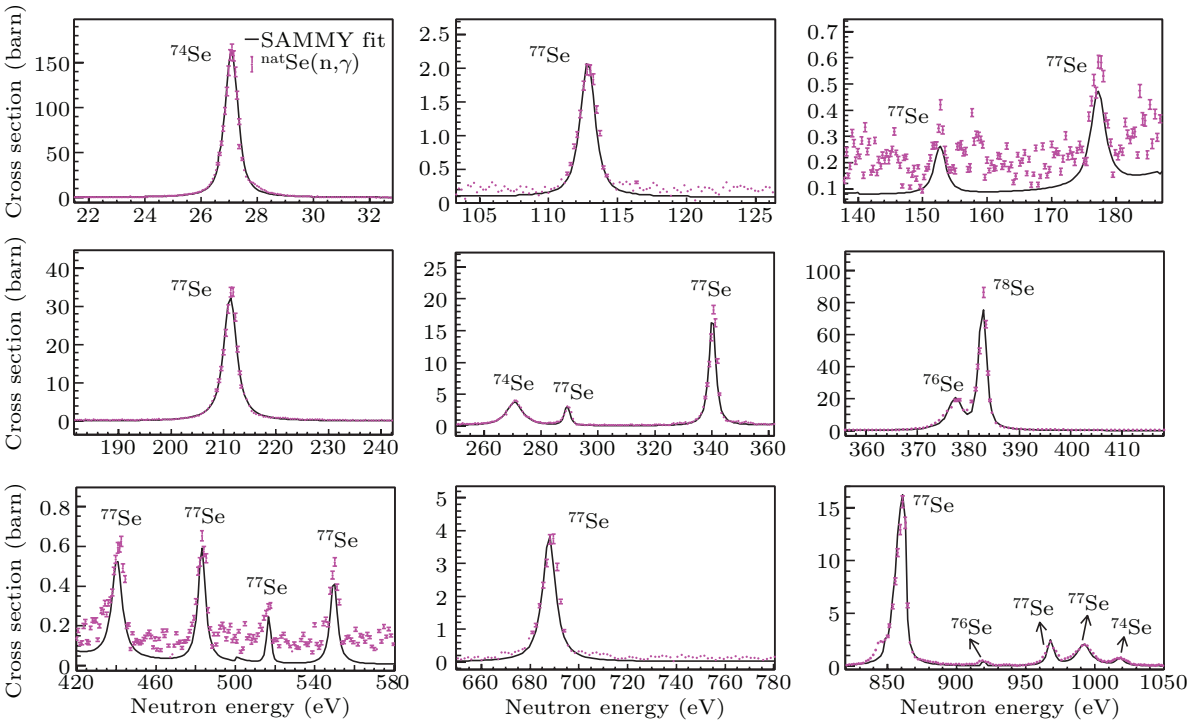

Fig. 9. The resolved resonance range of 1 eV to 1050 eV analyzed in this work. The pink points are the experimental data, and the black line is the *R*-matrix fit performed with SAMMY.

Neutron resonances up to about 1.05 keV neutron energy were identified and analyzed using the multilevel *R*-matrix code SAMMY.[38] The fitting procedure applied in the Reich–Moore approximation to find the "best fit" values of resonance parameters and the associated parameter covariance matrix was based Bayes's theorem. In the above 1050 eV, due to the limited energy resolution of the detection system, the *R*-matrix analysis was not performed. The fit included multiple scattering and self-shielding corrections, and Doppler broadening with an effective temperature of 300 K using the free gas model (FGM). Owing to many energy broadenings, the measured resonance widths were larger than the natural widths; and only the capture kernel could be determined. It is related to the resonance area via[41]

$$k_\gamma = \frac{2}{\pi\lambda^2}\int_{-\infty}^{+\infty}\sigma(E)\,\mathrm{d}E = g_\mathrm{s}\frac{\Gamma_\mathrm{n}\Gamma_\gamma}{\Gamma_\mathrm{n}+\Gamma_\gamma}, \tag{9}$$

where λ denotes the de Broglie wavelength at the resonance energy, and Γ_n, Γ_γ represent the neutron and gamma partial widths, respectively. The statistical spin factor g_s =

$(2J+1)/(2S+1)(2I+1)$ is determined by the resonance spin J, the neutron spin $S=1/2$, and the spin I of the target nucleus. And the resonance spin $\boldsymbol{J}=\boldsymbol{I}+\boldsymbol{S}+\boldsymbol{l}$ relates to the neutron orbital angular momentum $\boldsymbol{l}$, i.e., $l=0$ corresponding to s-wave neutron, $l=1$ to p-wave neutron. The resonance fits up to 1050 eV are shown in Fig. 9, which match the experimental data well. At last, we extracted the corresponding resonance parameters, i.e., the neutron width ($\Gamma_{\rm n}$) and gamma partial width (Γ_γ) seen in Table 3. We get three resonances for ^{74}Se contribution at 27.1 eV, 270.8 eV, and 1018 eV; and most of the resonances are of ^{77}Se nuclei's contribution. Since some of the nuclei ^{77}Se weighed resonance cross sections are relatively low, introducing increased background errors, the authors recommend measuring the neutron capture cross section of ^{77}Se isotope separately and extracting the corresponding resonance parameters.

Table 3. The resonance parameters above 27 eV obtained by this work. Quantum number I, l and J^π are taken from ENDF/B-VIII.0, and $E_{\rm R}$ represents the ENDF/B-VIII.0 evaluated resonance energy.

$E_{\rm Experiment}$ (eV)	$E_{\rm R}$ (eV)	Isotope	I	l	J^π	This work		ENDF/B-VIII.0	
						Γ_γ (meV)	$\Gamma_{\rm n}$ (meV)	Γ_γ (meV)	$\Gamma_{\rm n}$ (meV)
27.08	27.10	^{74}Se	0	0	$\frac{1}{2}^+$	242.9	146.5	210.0	170.0
112.8	112.0	^{77}Se	0.5	0	1^-	838.6	1.65	700.0	1.60
152.7	151.6	^{77}Se	0.5	1	0^+	547.4	0.559	380.0	0.760
177.4	176.4	^{77}Se	0.5	1	1^+	400.0	0.501	380.0	0.493
211.3	211.6	^{77}Se	0.5	0	0^-	463.8	2005.0	350.0	1520.0
270.8	271.5	^{74}Se	0	0	$\frac{1}{2}^+$	290.1	6004.4	300.0	4449.0
289.6	290.6	^{77}Se	0.5	0	1^-	382.0	8.29	380.0	12.2
340.7	340.8	^{77}Se	0.5	0	1^-	440.0	145.5	380.0	120.0
377.2	378.0	^{76}Se	0	0	$\frac{1}{2}^+$	244.0	299.6	240.0	300.0
382.7	383.0	^{78}Se	0	0	$\frac{1}{2}^+$	97.87	81.9	210.0	325.0
440.8	442.0	^{77}Se	0.5	1	0^+	389.1	7.51	380.0	17.40
483.4	482.0	^{77}Se	0.5	0	1^-	438.2	2.78	380.0	10.53
516.5	517.0	^{77}Se	0.5	1	2^+	422.6	1.10	380.0	2.00
549.6	552.0	^{77}Se	0.5	1	0^+	290.3	3.90	380.0	17.2
687.7	690.0	^{77}Se	0.5	0	0^-	345.7	5917.2	330.0	2380.0
861.7	864.0	^{77}Se	0.5	0	1^-	279.6	1691.5	380.0	613.3
918.4	920.0	^{76}Se	0	1	$\frac{1}{2}^-$	270.6	30.76	232.0	40.0
968.1	970.0	^{77}Se	0.5	0	1^-	561.4	165.8	380.0	126.7
992.0	997.0	^{77}Se	0.5	0	0^-	502.5	11325	450.0	7600.0
1018.0	1029.0	^{74}Se	0	0	$\frac{1}{2}^+$	206.2	6610.7	300.0	2371.0

5. Conclusion

For the first time, the $^{\rm nat}$Se neutron capture cross section in the 1 eV–100 keV energy region has been measured at the Back-n facility of CSNS by using the four C_6D_6 liquid scintillator detectors. A detailed description of data analysis with PHWT and system uncertainty evaluation are given. The cross sections in the 10–100 keV energy are a good agreement with the JENDL-4.0 and ENDF/B-VIII.0 evaluated data, which verify the correctness of the experimental method and data processing. Data in the 1 keV–10 keV energy range exist larger errors due to the large in-beam gamma background and the limitation of neutron energy discrimination at current experimental conditions. The data of the 1 eV–1050 eV were analyzed in detail and the R matrix program was used to provide the isotope contribution of the natural selenium resonance shape and the corresponding resonance parameters. The result shows that ^{74}Se and ^{77}Se isotopes have greater contributions on the resonance peaks of natural selenium in the 1–1050 eV energy region.

Data availability

The data that support the findings of this study are openly available in Science Data Bank at http://doi.org/10.11922/sciencedb.j00113.00019.

Acknowledgements

The authors sincerely appreciate the efforts of the staff of the CSNS and Back-n collaboration as well as Prof. Gui-Lin Zhang for his useful suggestion on data analysis. This work was supported by the National Natural Science Foundation of China (Grant Nos. 11875311, 11905274, 11705156, 11605097, and U2032146) and the Strategic Priority Research Program of Chinese Academy of Sciences (Grant No. XDB34030000).

References

[1] Kappeler F 1999 *Prog. Part. Nucl. Phys.* **43** 419
[2] Kappeler F, Gallino R, Bisterzo S and Wako Aoki 2011 *Rev. Mod. Phys.* **83** 157
[3] Qian Y Z 2003 *Prog. Part. Nucl. Phys.* **50** 153

[4] Kappeler F 2011 *Prog. Part. Nucl. Phys.* **66** 390

[5] Rauscher T, Dauphas N, Dillmann I, *et al.* 2013 *Rep. Prog. Phys.* **76** 066201

[6] Reifarth R, Lederer C and Kappeler F 2014 *J. Phys. G: Nucl. Part. Phys.* **41** 053101

[7] Larsen A C, Spyrou A, Liddick S N, *et al.* 2019 *Prog. Part. Nucl. Phys.* **107** 69

[8] Utsunomiya H, Hara K Y, Goko S *et al.* 2004 *Nucl. Phys. A* **738** 136

[9] Makinaga A, Utsunomiya H, Goriely S, *et al.* 2009 *Phys. Rev. C* **79** 025801

[10] Hermann Beer, Walter G and Kappeler F 1992 *Ap. J.* **389** 784

[11] Kamada S, Igashira M, Katabuchi T, *et al.* 2010 *J. Nucl. Sci. Techn.* **47** 634

[12] Babiano-Suarez V, *et al.* 2020 *J. Phys.: Conf. Ser.* **1668** 012001

[13] Chen H S and Wang X L 2016 *Nat. Mater.* **15** 689

[14] An Q, Bai H Y, Bao J, *et al.* 2017 *J. Instrum.* **12**, P07022

[15] Jing H T, Tang J Y, Tang H Q, *et al.* 2010 *Nucl. Instrum. Methods A* **621** 91

[16] Tang J Y, Bai J B, *et al.* 2021 *Nucl. Sci. Tech.* **32** 11

[17] Tang J Y and the CSNS Back-n Collaboration 2019 *Proceeding of ND2019, EPJ Web of Conferences* **239** 06002

[18] Li X X, Liu L X, Jiang W, *et al.* 2020 *Nucl. Tech.* **43** 80501 (in Chinese)

[19] Li X X, Liu L X, Jiang W, *et al.* 2022 *Chin. Phys. B* **3** 038204

[20] Ren J, Ruan X C, Bao J, *et al.* 2019 *Radiat. Detect. Technol. Methods* **3** 52

[21] Wang Q, Cao P, Qi X, *et al.* 2018 *Rev. Sci. Instrum.* **89** 013511

[22] Li Q, Luan G Y, Bao J, *et al.* 2019 *Nucl. Instrum. Methods A* **946** 162479

[23] Macklin R L, Halperin J and Winters R R 1979 *Nucl. Instrum. & Methods* **164** 213

[24] Reifarth R, Erbacher P, Fiebiger S, *et al.* 2018 *Eur. Phys. J. P* **133** 424

[25] Moxon M C and Rae E R 1963 *Nucl. Instr. and Meth.* **24** 445

[26] Macklin R L and Gibbons J H 1967 *Phys. Rev.* **159** 1007

[27] Borella A, Aerts G, Gunsing F, *et al.* 2007 *Nucl. Instr. Method A* **577** 626

[28] Hu X R, Fan G T, Jiang W, *et al.* 2021 *Nucl. Sci. Tech.* **32** 101

[29] Li X X, Liu L X, Jiang W, *et al.* 2021 *Phys. Rev. C* **104** 054302

[30] Fraval K, Gunsing F, Altstadt S, *et al.* 2014 *Phys. Rev. C* **89** 044609

[31] Lerendegui M J, Guerrero C, Mendoza E, *et al.* 2018 *Phys. Rev. C* **97** 024605

[32] Chen Y H, Luan G Y, Bao J, *et al.* 2019 *Eur. Phys. J. A* **55** 115

[33] Tain J L, Gunsing F, Daniel aniel-Cano, *et al.* 2002 *Journal of Nuclear Science and Technology* **39** 689

[34] Ren J, Ruan X C,Jiang W, *et al.* 2021 *Nucl. Instrum. Methods A* **985** 164703

[35] Sirakov I, Kopecky S and Yong P G http://www-nds.iaea.org/exfor/endf.htm

[36] Iwamoto N http://www-nds.iaea.org/exfor/endf.htm

[37] Koning A J and Rochman D http://www-nds.iaea.org/exfor/endf.htm

[38] Larson N M *Updated Users' Guide for SAMMY: Multilevel R-matrix Fits to Neutron Data Using Bayes' Equations*, Oak Ridge National Laboratory Report No.ORNL/TM-9179/R6

[39] Macklin R L, Gibbons J H and Inada T 1962 *Phys. Rev.* **129** 6

[40] Belanova T S *Measurements of the absorption cross section for fast neutrons*, *Zhur. Eksptl'. i Teoret. Fiz.*

[41] Lederer C, Massimi C, Berthoumieux E, *et al.* 2014 *Phys. Rev. C* **89** 025810